

A Paradigm Shift for Preparing Versatile M^{2+} -Free Gels from Unmodified Sodium Alginate

*Maria M. Pérez-Madrigal,^{a,b,c} Joan Torras,^{b,c} Jordi Casanovas,^d Marleen Häring,^a Carlos Alemán^{*b,c} and David Díaz Díaz^{*a,e}*

^aInstitut für Organische Chemie, Universität Regensburg, Universitätsstr. 31, D-93053 Regensburg, Germany. ^bDepartament d'Enginyeria Química, EEBE, Universitat Politècnica de Catalunya, C/ Eduard Maristany, 10-14, Ed. I2, 08019, Barcelona, Spain. ^cBarcelona Research Center in Multiscale Science and Engineering, Universitat Politècnica de Catalunya, C/ Eduard Maristany, 10-14, 08019, Barcelona, Spain. ^dDepartament de Química, EPS, Universitat de Lleida, Jaume II 69, 25001 Lleida, Spain. ^eIQAC-CSIC, Jordi Girona 18-26, E-08034 Barcelona, Spain

ABSTRACT. This manuscript describes a new route to prepare rapidly Ca^{2+} -free hydrogels from unmodified sodium alginate by simply mixing with small organic molecules such as polycarboxylic acid compounds as cross-linker agents instead of classical divalent metal salts such as $CaCl_2$. DMSO was also found to induce the rapid gelation of aqueous alginate solutions. The gelation process takes place at RT and depending on the composition, gels with good thermal (90-100 °C) and mechanical properties compared to classical metal-containing analogs

are obtained. DMSO-based gels showed remarkable self-supporting and thixotropic properties, which can be tuned by the biopolymer concentration. Furthermore, oxalic-based gels showed superior elasticity than HCl, CaCl₂ and DMSO-based gels. The possibility to prepared monoliths, beads and films of these gels provide them significant versatility. In particular, films made of alginate and oxalic acid showed good potential as synergistic anticancer drug delivery carrier. Computational studies using both quantum mechanical and classical force-field methodologies revealed that hydrogen bonding networks between water and DMSO molecules located close to the alginate chains are responsible of the stability of DMSO-based gels. In contrast, the cohesion of oxalic-based gels is due to the coexistence of multiple ionic associations involving oxalate, alginate and Na⁺ counterions, which stabilize the system and keep all the interacting species grouped.

INTRODUCTION

Over the years, naturally occurring polymers have been extensively investigated in biomaterials science due to their biocompatibility, low toxicity, relatively low cost and gelation properties. Among them, alginate has emerged as one of the most reliable and versatile anionic biopolymer in industry. It is typically obtained from brown algae (*Phaeophyceae*)¹ by alkali treatment with NaOH.² After filtration, NaCl is added to the filtrate affording the precipitation of sodium alginate (Na-Alg), which can be also converted into insoluble alginic acid upon protonation of pendent acidic groups by treatment with dilute HCl.³⁻⁵ From the structural point of view, alginates⁶⁻⁸ are biocompatible and biodegradable linear copolymers with homopolymeric blocks of (1,4)-linked β -D-mannuronate (M) and its C-5 epimer α -L-guluronate (G) residues,

respectively, covalently linked together in different sequences. The monomers can appear in homopolymeric blocks of consecutive G-residues (G-blocks), consecutive M-residues (M-blocks) or alternating M- and G-residues (MG-blocks). Depending on the source, alginates differ in both the M/G ratio and the length of each block.⁹ The molecular weight of commercially available sodium alginate ranges between 32,000 and 400,000 g/mol, and the viscosity of their solutions increase as pH decreases, reaching a maximum around pH 3–3.5, as carboxylate groups in the alginate backbone become protonated and form hydrogen bonds.¹⁰

Alginate is typically used in the form of cross-linked hydrogels in biomedicine, mainly for wound healing, *in vitro* cell culture, drug delivery and tissue engineering applications.¹¹ Different strategies have been developed for the cross-linking of alginate chains allowing for the preparation of hydrogels with tunable physical properties. These approaches include, for instance, formation of semi-interpenetrating polymer networks via *in situ* copolymerization of alginate and *N*-isopropylacrylamide (NIPAAm),¹² formation of alginate-pectinate complexes,¹³ cell cross-linking of RGD-modified alginates,^{14,15} combination of alginates with magnesium aluminum silicates,¹⁶ photo cross-linking of methacrylate-modified alginates,^{17,18} covalent cross-linking of alginates with glutaraldehyde¹⁹ or diamines via carbodiimide chemistry,²⁰ covalent cross-linking of partially oxidized alginates with dihydrazides²¹ and oxidative cross-linking of covalently conjugated alginate-dopamine.²² However, the most common method to prepare hydrogels from aqueous alginate solutions is the ionic cross-linking in the presence of divalent cations, typically Ca^{2+} . These cations are believed to bind solely to the carboxylic groups of the G-blocks of two adjacent polymer chains forming stable conformations with junction zones affording a 3D gel network. This has been classically described as the “egg-box” model of cross-linking to explain the formation of alginate hydrogels (Figure 1),²³⁻²⁵ which has been supported

by a series of molecular dynamics and semiempirical studies.^{26,27} Furthermore, Plazinski²⁸ has also proposed the possibility of alternative structural models of Ca^{2+} -polyguluronate complexes where Ca^{2+} ions are coordinated by four oxygen atoms from two opposite carboxyl groups of two polyguluronate chains and, additionally, by four oxygen atoms belonging to water molecules.

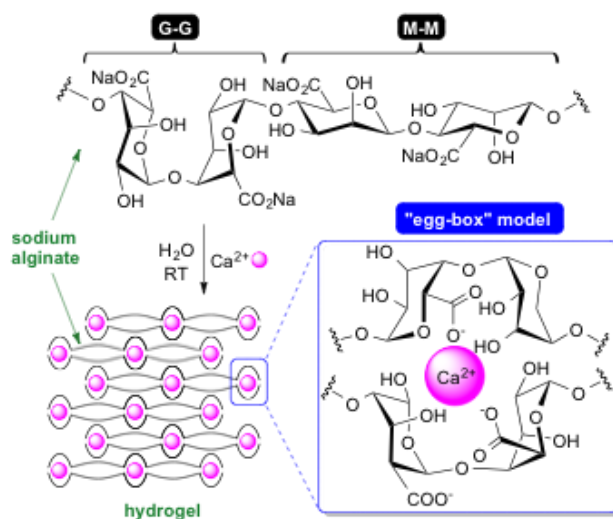


Figure 1. Conventional method for the preparation of alginate hydrogels by ionic cross-linking of Na-Alg with Ca^{2+} ions. Only guluronate (G) blocks participate in the formation of a corrugated “egg-box”-like structure with Ca^{2+} ions located at the interstices.

In this work, we demonstrate for the first time that Ca^{2+} -free hydrogels can be prepared from Na-Alg by simple addition of small organic molecules such as dimethyl sulfoxide (DMSO) or oxalic acid as cross-linker agents without any chemical modification of the biopolymer backbone. The specific role of the mentioned organic additives in the gelation mechanism, which at first glance may seem counterintuitive, has also been rationalized with the aid of quantum mechanical calculations and molecular dynamics simulations. To the best of our knowledge, the use of DMSO in alginate-containing formulations has been limited so far to cell

cryopreservation^{29,30} and as solution media for chemical modifications.³¹ Moreover, hydrogels made of alginate and oxalic acid showed great potential as synergistic anticancer drug delivery carrier.

EXPERIMENTAL SECTION

Materials

Alginic acid sodium salt from brown algae was purchased from Sigma-Aldrich (low viscosity, A2158). Methotrexate hydrate (MTX) was purchased from TCI Europe (M1664, CAS 59-05-2). Unless otherwise noted, the rest of chemicals and solvents were also purchased from commercial suppliers and used without further purification.

Procedure for the preparation of M²⁺-free alginate gels

Aqueous solutions of Na-Alg at different % w/v were prepared by dissolving the corresponding amount of Na-Alg in H₂O at ca. 50 °C. The obtained viscous solutions (from transparent to yellow-colored, depending on the biopolymer concentration) were allowed to cool down to room temperature (RT) without control of the cooling rate. The appropriate amount of DMSO was added using a micropipette on top of the Na-Alg solution (1 mL) placed in a vial. The mixture was stirred gently with a spatula for a few seconds and subsequently submitted to ultrasound for 5 min. After this time, the system was let to gel at RT for at least 24 h. The specificity of DMSO to induce the formation of hydrogels using Na-Alg was evaluated by replacing DMSO with a) other organic solvents having similar solvatochromic parameters or b) small organic molecules dissolved in water. The volume of solvent/solution added to the Na-Alg aqueous solution and the biopolymer concentration were selected as input variables in this study.

On the other hand, Na-Alg hydrogel beads were prepared by dropping 3 mL of a 2% w/v

or 4% w/v Na-Alg solution via an addition funnel into the desired cross-linker solution. The tip of the addition funnel (inner diameter = 0.5 cm) was placed at a distance of ca. 1 cm above the surface of the cross-linker solution. Approximately, 30–35 beads were obtained in each case, and were matured in the cross-linker solution for 30 min. So obtained beads were thoroughly washed with water (at least 8×250 mL) to a neutral pH and stored in water inside a sealed vial at 4 °C before their characterization.

Note: Addition of DMSO to water at 22 °C increases the temperature of the mixture until 44 °C ($\Delta T = 22 \pm 2$ °C). Similarly, the addition of DMSO to the aqueous alginate solution (2%) increases the temperature of the mixture until 40 °C ($\Delta T = 18 \pm 2$ °C).

Preparation of drug-loaded gel scaffolds

Na-Alg/oxalic acid-based gels, beads and films were prepared with a loaded anticancer MTX to test their application as drug delivery systems. Moreover, analogues gel systems cross-linked with CaCl_2 were also prepared for comparison. A summary of the different materials prepared is given next:

a) Control Na-Alg hydrogel films were cast from sodium alginate solutions, which were prepared at 2 and 4% w/v by dissolving the corresponding amount of sodium alginate powder in water at 50 °C. Films on glass substrates (3.7 cm in diameter) were prepared by solvent casting Na-Alg solution (1.3 mL) and subsequent drying overnight at RT. After that period, the casted films were easily peeled off from the mold, and cut in pieces of approximately 1×1 cm. Then, each alginate piece was cross-linked by a one-step procedure. The sample was completely immersed in the cross-linker solution (30 mL in either 0.1 M CaCl_2 or 0.5 M oxalic acid solution) for 5 min. After this time, the films were rinsed manually several times in water to

dissolve any remaining salt adhered to the surface. The films were dried overnight at RT, and stored in closed vials at RT prior characterization. Note: Na-Alginate films were not possible to cross-link in DMSO. Instead of gelation, the film was dissolved within 1 min in the organic solvent.

b) Control Na-Alg hydrogel beads were prepared by dropping Na-Alg solution (3 mL from a 2% w/v solution) into the cross-linker solution (0.1 M CaCl₂ or 0.5 M oxalic acid solution).

c) Control Na-Alg gels were prepared by adding oxalic acid (0.3 mL from a 0.5 M solution) or CaCl₂ (0.3 mL from a 0.1 M solution) onto Na-Alg aqueous solution (1 mL from a 2% w/v solution).

d) Drug-loaded hydrogel samples (gels, films and beads) were prepared following the above-described procedure but using Na-Alg aqueous solutions containing MTX. Specifically, MTX (20 mg) was dissolved in a H₂O:EtOH mixture (5 mL, 3:1 v/v) and submitted to ultrasound to facilitate drug dissolution. Then, the MTX-containing solution was added to a Na-Alg aqueous solution (5 mL, 4% w/v), and mixed using a magnetic stirring bar. Furthermore, to ensure the minimum MTX loss during the formation of the beads, the curing time was reduced to 10 min, and MTX-containing beads were only washed with water (2 × 250 mL).

Drug-release studies from bulk gels, beads and films

Alg-MTX gel materials were allowed to equilibrate for 24 h prior to drug release experiments. After this time, Alg-MTX gels were overlaid with phosphate-buffered saline (PBS, 1 mL, pH 7.4), and incubated at room temperature. In the case of films and beads, each piece of film (1 cm × 1 cm) or bead was placed into an Eppendorf tube and immersed in PBS (1 mL). At selected time points, aliquots (100 µL) were removed and diluted with PBS to 1 mL. Then, fresh PBS (100 µL) was added over the gel material to maintain infinite sink conditions. Drug concentration

in the aliquots was determined using UV-spectroscopy after proper calibration using the maximum absorbance of MTX at 305 nm or 351 nm depending on the system as explained in the results section (see main paper). Samples were centrifuged (EBA 12 Hettich Zentrifugen) at 4000 rpm for 5 min before measurements. The experiments were carried out in triplicate and average values are reported. Moreover, both the cross-linking and the curing solutions, as well as the washing aqueous solutions were also analyzed by UV-vis to check any possible MTX loss during the preparation of the films and beads. UV-vis spectroscopy was performed using a Varian Cary 50 UV spectrophotometer and quartz-glass cuvettes of 0.5 cm thickness. The results were plotted after applying the corresponding correction derived from withdrawing aliquots and further replacement by an equivalent volume of solvent.

Characterization of gel-based materials

Gel-to-sol transition temperatures (T_{gel}) values were determined by the dropping ball method. Gels (total volume = 1.3 mL for Alg/acid or 2 mL for Alg/DMSO systems) were prepared in clear glass vials. After an equilibration time of 24 h, a glass ball (285 mg) was placed on top of the gel, and the vials were placed into a mold of an alumina block and heated up using an electric heating plate equipped with a temperature control coupled to an oil bath.³² Herein, T_{gel} was defined as the temperature at which gel material collapsed and the ball fell to the bottom of the vial. The values were verified by differential scanning calorimetry (DSC) measurements that were performed on a Mettler Toledo Differential Scanning Calorimeter using a DSC 30 measuring cell. The DSC thermograms were obtained under dynamic argon atmosphere (gas flow rate = 25 mL/min) at a heating rate of 10 °C/min. Samples were placed in closed aluminum pans (Mettler Toledo). An empty sample holder was used as reference and the runs were performed by heating the samples from 20 to 90 °C at 10 °C/min with an initial stabilization

period of 1 min at 20 °C/min and a final period of 5 min at 90 °C. The samples were subsequently cooled from 90 to 20 °C at 10 °C/min.

The morphology of the samples (xerogels) was examined by scanning electron microscopy (SEM) using a Focused Ion Beam Zeiss Neon40 scanning electron microscope equipped with an energy dispersive X-ray (EDX) spectroscopy system and operating at an accelerating voltage of 5 kV. All samples were sputter-coated with a thin carbon layer of 6–10 nm thickness using a K950X Turbo Evaporator to prevent electron charging problems. The specimens were prepared by the freeze-drying method (i.e., an Eppendorf tube (1 mL) containing a piece of the gel was frozen in liquid nitrogen and subsequently evaporated under reduced pressure overnight at room temperature).

FT-IR absorption spectra of freeze-dried samples were recorded on a FT-IR Jasco 4100 spectrometer. Samples (either powder or xerogels obtained by the above described freeze-drying method) were placed on an attenuated total reflection accessory (top plate) with a diamond crystal (Specac model MKII Golden Gate Heated Single Reflection Diamond ATR). For each sample, 32 scans were performed between 4000 and 600 cm^{-1} with a spectral resolution of 4 cm^{-1} .

Dynamic oscillatory rheological measurements of the gels were performed with an AR 2000 rheometer (TA instruments) equipped with a cooling system (Julabo C) using 40 mm flat plate geometry (stainless steel) and a gap size of 0.5 mm at 25 °C. Evolution of the storage (G') and loss (G'') moduli was studied as following: Dynamic strain sweep (DSS) measurements were first performed between 0.1% and 100% strain at 1 Hz frequency to establish the strain value at which reasonable torque values were given (about 10 times of the transducer resolution limit). Subsequently, dynamic frequency sweep (DFS) measurements (from 0.1 to 10 Hz at 0.1% strain)

and time sweep measurements (DTS) within the linear viscoelastic regime (0.1% strain and 1 Hz frequency) were carried out. Furthermore, the thixotropic properties of the gels were investigated by loop experiments consisting in the following steps: (1st step) Application of a low shear strain (0.1% and 1 Hz frequency, gel phase: $G' > G''$), (2nd step) increase of the shear strain (1000%) until the gel breaks (viscous solution phase, $G' < G''$), and (3rd step) return at the same rate to the initial strain % value (recovered gel phase, $G' > G''$). The loop was repeated two times.

Simulation studies

Quantum mechanical calculations. Density Functional Theory (DFT) calculations on model compounds were performed using the Gaussian 09 computer package.³³ The geometries of the different investigated systems were fully optimized using the M06L^{34,35} functional, which was developed by Zhao and Truhlar to account for dispersion, combined with the 6-31+G(d,p) basis set. No symmetry constraints were used in the geometry optimizations. All geometry optimization were performed in both the gas-phase and aqueous solution. For the latter, the solvent was described as a dielectric medium using a well established Self-Consistent Reaction Field (SCRF) method, that is, the Polarizable Continuum Model (PCM) of Tomasi and co-workers.³⁶

Molecular dynamics (MD) simulations. All classical simulations were carried out using the AMBER 14³⁷ software and the potential energy function of AMBER.³⁸ Force-field parameters for the Na-Alg were taken from the GLYCAM06 libraries.³⁹ Water molecules were represented by the TIP3P model,⁴⁰ while data for DMSO were taken from the parametrization developed by Fox and Kollman for organic solvents.⁴¹ Finally, oxalic acid in its protonated, partially deprotonated and completely deprotonated forms were described using the GAFF

parameters.⁴² In all cases, the negative charges of the carboxylate groups of Na-Alg and deprotonated oxalic acid molecules were neutralized with Na⁺ ions.

Bond lengths involving hydrogen atoms were kept at their equilibrium distances using the SHAKE algorithm.⁴³ Atom pair distance cutoffs were applied at 15.0 Å to compute the van der Waals interactions. Electrostatic interactions were extensively computed by means of Ewald summations.⁴⁴ The real space term was defined by the van der Waals cutoff (15.0 Å), while the reciprocal space was computed by interpolation of the effective charge into a charge mesh with a grid thickness of 5 points per volume unit (particle mesh Ewald).

Na-Alg-DMSO gels were investigated using three different models, Na-Alg being described in both cases by two G-blocks of six residues each and 12 Na⁺. Thus, differences between such three models, hereafter denoted Na-Alg-DMSO/# are the following:

- **Na-Alg-DMSO/1** contained 3 DMSO molecules at the cavity between the two chains (see Figure S17), and 2296 explicit water molecules.

- **Na-Alg-DMSO/2** involved a total of 576 DMSO molecules (3 at the cavities between the two modelled Na-Alg chains) and 2288 water molecules (50:50 w/w) randomly distributed.

- **Na-Alg-DMSO/3** accommodated 629 DMSO molecules, without additional water molecules.

On the other hand, Na-Alg-oxalic gels were initially studied using three model systems, which essentially differ in the protonation degree of oxalic acid and its concentration:

- **Na-Alg-Ox²⁻/1** contained 3 oxalate dianions (Ox²⁻) located at the cavity defined by the two Na-Alg chains, 18 Na⁺, and 2455 explicit water molecules.

- **Na-Alg-Ox²⁻/2** formed by 20 Ox²⁻, 2 Na-Alg chains, 52 Na⁺, and 4350 explicit water molecules.

- **Na-Alg-OxH⁻** involved 3 hydrogen oxalate anions (OxH⁻) located at the cavity defined by the two Na-Alg chains, 15 Na⁺, and 2401 explicit water molecules.

Models for both Na-Alg-DMSO and Na-Alg-oxalic gels were constructed considering both the parallel and antiparallel arrangements of the Na-Alg chains. However, features provided by MD simulations were in all cases independent of the relative disposition of the biopolymer chains and, therefore, only results obtained for the parallel disposition are discussed in the next section. This feature is fully consistent with previous computational studies on Ca²⁺-Alg systems.⁴⁵

Each model was submitted to 5000 steps of energy minimization (conjugate gradient method) before any MD trajectory was run in order to relax conformational and structural tensions. The temperature and pressure of each model were equilibrated at 298 K and 1 bar, respectively, by two consecutive MD runs: 1) a NVT-MD simulation was run at 298 K for 0.1 ns; 2) a NPT-MD simulation was run at 298 K for 0.5 ns. In both cases the Na-Alg molecules were restrained at their initial positions. Both temperature and pressure were controlled by the Langevin dynamics and the Berendsen barostat⁴⁶ Pressure was kept at 1.01325 bars, the oscillation period was set at 2 ps while the collision rate was set at 3 ps⁻¹. The piston temperature was set at the same value as the thermostat control, 298 K, which used a damping coefficient of 2 ps. The integration step was 1 fs in all production simulations.

The most stable Na-Alg-DMSO/# model was studied using replica exchange MD (REMD). In order to ensure a reasonable replica swaps ratio of acceptance, 32 replicas were exponentially distributed in the temperature range from 272.00 K to 400.94 K. Exchanges were attempted every 0.4 ps between all neighbouring replicas with an average success ratio of ~0.35. The REMD trajectories resulted in a cumulative simulation time of 128 ns. Between replica

exchanges, the system was evolved using NVT Berendsen MD with a damping coefficient of $\gamma = 2.5 \text{ ps}^{-1}$ and an integration step of 2 fs. The replicas were previously equilibrated by a set of short runs (isothermal and isobaric equilibration), and completed with a final NVT run of 0.5 ns to ensure that each replica reached the target temperature. Atom pair distance cut-offs were applied at 10.0 Å to compute the van der Waals and electrostatic interactions. Bond lengths involving hydrogen atoms were constrained using the SHAKE algorithm.⁴³

RESULTS AND DISCUSSION

Na-Alg gelation induced by DMSO

During the development of different biopolymer-based conductive hydrogels,⁴⁷ we found by serendipity the unexpected gelation of Na-Alg aqueous solutions after adding a DMSO solution containing a conductive polymer. The atypical absence of Ca^{2+} in the gel mixture, motivated us to investigate the origin of the gelation process. Preliminary experiments showed that the conductive polymer was not playing any role on the gelation, which took place simply by mixing the Na-Alg solution and DMSO. In order to investigate the exact role of DMSO in the gelation process,⁴⁸⁻⁵⁰ different amounts of the solvent, from 0.1 to 1.2 mL, were added at RT to 1 mL of Na-Alg aqueous solutions ranging from 2 to 8 % w/v (Table 1 and Figure S1).

Table 1. Gelation ability of DMSO added onto 1 mL of Na-Alg aqueous solution (assessed after 24 h).^a

Na-Alg (% w/v)	Volume of DMSO added (mL)												
	0.1	0.2	0.25	0.3	0.4	0.5	0.6	0.7	0.8	0.9	1.0	1.2	
2	L	L	L	L	L	L	L ^c	L	L	G ^b	G	G	

3	L	L	L	L	L	G ^b	G ^b	G	G	G	G	G
4	L	L	L	G ^b	G	G	G	G	G	G	G	G
5	L	L	G ^b	G	G	G	G	G	G	G	G	G
8	L	G ^b	G	G	G	G	G	G	G	G	G	G

^aL = viscous liquid; G = transparent gel. ^bWeak gel. ^cVolume of DMSO = 0.65

mL.

Interestingly, the concentration of Na-Alg necessary to obtain stable gels decreased with increasing DMSO volume. As the mixing of DMSO and water is exothermic (−54 cal/g at 25 °C), the vials were noticed to warm up rapidly upon addition of DMSO (see Experimental Section). Moreover, bubbles were generated during the gelation process and were trapped inside the transparent gels (Figure 2). Application of ultrasound to the gels for *ca.* 10 min allowed the removal of the bubbles for the lowest concentration of Na-Alg (2% w/v). At higher concentrations of the biopolymer, bubbles either stayed on the top half of the gel, or were not able to diffuse at all due to the enhanced consistency of the gel. The gels were considered stable when no gravitational flow was observed upon inversion of the glass vial, and their nature was subsequently confirmed by dynamic rheological measurements. Interestingly, most gels could be destroyed by vigorous stirring with a spatula and restored upon resting overnight (Table S1). Such thixotropic behavior was also supported by loop-rheological experiments (*vide infra*, physicochemical characterization).

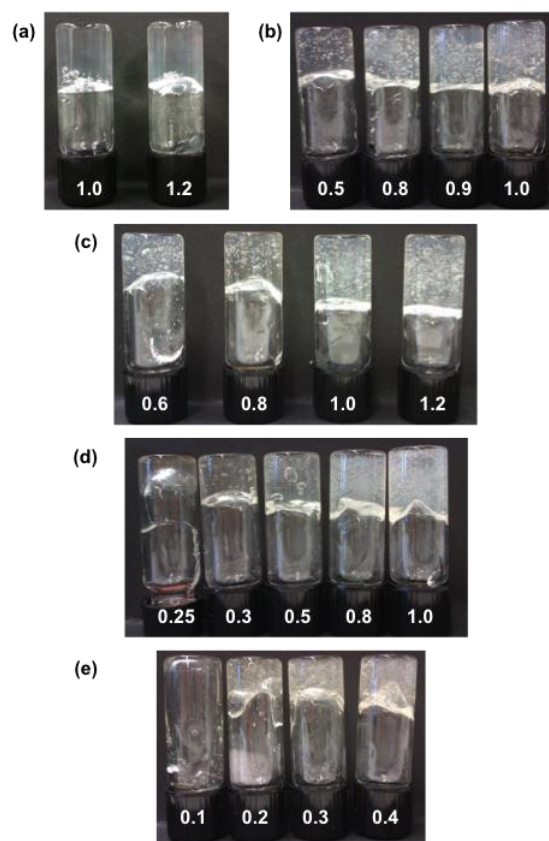


Figure 2. Representative digital photographs of gels obtained by adding different amounts of DMSO (values in mL are indicated in white) onto 1 mL of Na-Alg aqueous solutions prepared at: (a) 2% w/v, (b) 4% w/v, (c) 3% w/v, (d) 5% w/v and (e) 8% w/v.

Unless otherwise indicated, further studies were made with gels prepared using 1 mL of DMSO and 1 mL of Na-Alg solution at the indicated concentration (x% w/v). From now on, and for simplicity, these gels are denoted as Na-Alg (x%)-DMSO. Among the gels described in Table 1, Na-Alg (2%)-DMSO could be turned into a viscous fluid by heating with a heat gun until the first bubble appeared, and then mixed with a spatula. Fluid-to-gel transition took place upon cooling down the sample to RT. In contrast, the same procedure (heating + mixing) applied to gels made at higher concentrations (3 and 4%) led to incomplete gel-to-fluid transition. Nevertheless, the systems reverted to gels after resting overnight (Figure S2). The

thermoreversible and thixotropic nature of Na-Alg (2%)-DMSO also permitted the gel to be injected to a second vial through a syringe and restored overnight under undisturbed conditions (Figure 3). Transferring was more difficult and incomplete for higher concentrations of Na-Alg, although gelation was observed for the amount of material transferred to the second vial (Figure S3).

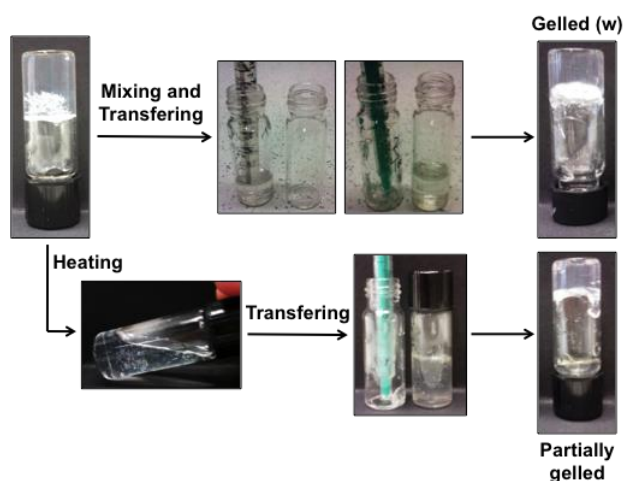


Figure 3. Injectability test for Na-Alg (2%)-DMSO gel. (w) refers to weak gel.

Finally, Na-Alg (2%)-DMSO and Na-Alg (4%)-DMSO gels were used to demonstrate the firmness of monoliths prepared inside syringes (with the tip cut off) instead of vials. After 24 h, the monoliths were easily pulled off from the syringes and placed on a glass surface. As it can be observed in Figure 4, Na-Alg (4%)-DMSO gel could support its own weight and form a bridge between two vials. In contrast, Na-Alg (2%)-DMSO gel spread quickly over the surface after being released from the syringe (Figure S4).

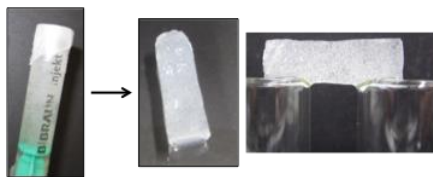


Figure 4. Self-sustainability test for Na-Alg (4%)-DMSO gel.

Specificity of DMSO for the gelation of Na-Alg solutions

The specificity of DMSO to induce the gelation of Na-Alg aqueous solutions was first assessed by using different solvents. For these experiments, 1 mL of each solvent was added to 1 mL of 2% w/v or 4% w/v Na-Alg aqueous solution, and the mixture stirred gently with a spatula followed by 5 min of ultrasound. The materials were left undisturbed overnight before any analysis. A series of solvents characterized by different solubility parameters were selected for this study, including other polar aprotic solvents (*i.e.*, dimethylformamide (DMF), dimethylacetamide (DMAC), *N*-methylpyrrolidone (NMP), diethylformamide (DEF), tetrahydrofuran (THF), acetone, acetonitrile) and polar protic solvents (*i.e.*, methanol (MeOH), ethanol (EtOH)). The results indicated that a stable Na-Alg (2%) gel could be formed only in DMF, and partial gelation occurred in acetone. On the other hand, for Na-Alg (4%), stable gels were obtained in DMF, and weak gels in NMP, DMAC, MeOH and EtOH, whereas partial or no gelation was obtained when using acetone and DEF, or THF and CH₃CN, respectively (Table S2, Figure S5 and Figure S6). It should be emphasized that the gels obtained by adding other organic solvents support the inversion of the vial, but they flow down under vigorous agitation.

Considering that DMSO could in some way act as cross-linker between alginate chains, we anticipate that other small coordinating water-soluble molecules would behave similarly. Thus, to evaluate this possibility we tested L-arginine (0.5 M), *N*-methyl urea (0.5 M and 1 M)

and oxalic acid (0.5 M) as alternative gelation-inducing additives. No gels could be obtained with L-arginine or *N*-methyl urea in 4% w/v Na-Alg. However, oxalic acid exhibited very good gelation induction. Specifically, 0.3 mL of oxalic acid (0.5 M, pH = 1.0) promoted gelation when added to 1 mL of either 2% w/v or 4% w/v Na-Alg solution (Figure 5a). In contrast to DMSO, the gels obtained with oxalic acid did not show thermal gel-to-fluid transition. Interestingly, no gelation was observed when adding 0.3 mL of acetic acid (0.5 M) or 1 mL of ethylene glycol to 1 mL of 4% w/v Na-Alg solution (Figure S7). These results suggest the influence of the dicarboxylic acid as a cross-linking agent in the gelation mechanism. This was supported by the successful use of other di- and tri-functional carboxylic acid compounds, *i.e.*, maleic acid (0.5 M, pH = 1.0, *in situ* formation of maleic acid was achieved by slow but progressive hydrolysis of the anhydride⁴⁷), tartaric acid (0.5 M, pH = 1.5), glutaric acid (2.0 M, pH = 2.0) and citric acid (0.5 M, pH = 1.0). Figure 5 shows representative photographs of the gels obtained by adding the above acids. The gels that showed higher *gel-to-sol* transition temperature ($T_{gel} = 90\text{--}100\text{ }^{\circ}\text{C}$) were obtained with oxalic acid and maleic acid (Table S3). All these gels displayed different degree of opacity. The use of organic acids as cross-linkers for the gelation of other systems has also been recently reported.⁵¹⁻⁵³ Besides, considering the very low pH of all solutions, we wondered if we could induce the gelation of Na-Alg by simple combination with a strong inorganic acid such as HCl. However, attempts to achieve bulk gelation by mixing 1 mL of 2% or 4% w/v Na-Alg solutions and 0.3 mL of 1 M HCl yielded inhomogeneous gels combined with non-gelled fluid.

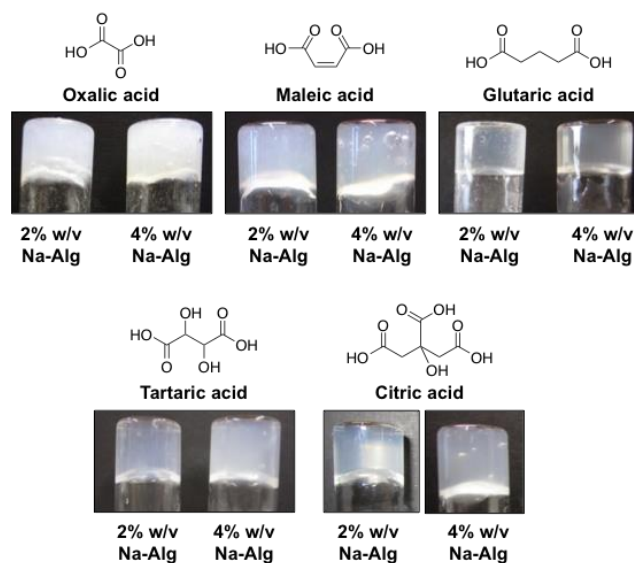


Figure 5. Representative digital photographs of gels obtained by adding 0.3 mL of 0.5 M acid solutions onto 1 mL of Na-Alg aqueous. Solutions prepared at 2% w/v and 4% w/v as indicated. Only for glutaric acid the concentration was adjusted to 2 M.

Finally, one of the most important properties of Ca^{2+} -alginate hydrogels for different applications is that they can be easily processed in different forms such as beads or films. With this in mind, uniform and spherical beads could be also obtained by adding dropwise 4% w/v Na-Alg solution onto the oxalic acid solution (0.5 M) (Figure 6a). These beads remained stable for at least five weeks in a closed vial. It is worth mentioning that beads were also obtained in DMSO, albeit they were more irregular and significantly less stable during neutralization washing than those obtained with oxalic acid (Figure S8 and Table S4). The use of citric acid (0.5 M) and maleic acid (0.5 M) also allowed the preparation of spherical beads. In contrast, glutaric acid (2 M) and tartaric acid (0.5 M) were ineffective as bead-forming solutions, whereas 4% w/v Na-Alg solution added dropwise onto a 1M HCl solution led to uniform and spherical beads (Figure S9).



Figure 6. Na-Alg beads (4% w/v) obtained by dropwise addition in 0.5 M oxalic acid. Beads were washed with water several times (picture in the middle).

Physicochemical characterization of model gels

For comparison reasons, we selected the following representative gels for further characterization. All gels were prepared as described above:

(1) Gelation induced by DMSO:

- Na-Alg (2%)-DMSO = 1 mL 2% w/v Na-Alg + 1 mL DMSO (gel)

- Na-Alg (4%)-DMSO = 1 mL 4% w/v Na-Alg + 1 mL DMSO (gel)

(2) Gelation induced by oxalic acid:

- Na-Alg (2%)-oxalic-gel = 1 mL 2% w/v Na-Alg + 0.3 mL oxalic acid (0.5M)

- Na-Alg (2%)-oxalic-beads = 2% w/v Na-Alg beads in oxalic acid (0.5M)

(3) Gelation induced by CaCl₂:

- Na-Alg (2%)-CaCl₂-gel = 1 mL 2% w/v Na-Alg + 0.3 mL CaCl₂ (0.5M)

- Na-Alg (2%)-CaCl₂-beads = 2% w/v Na-Alg beads in CaCl₂ (0.1M)

(4) Gelation induced by HCl:

- Na-Alg (2%)-HCl-gel = 1 mL 2% w/v Na-Alg + 0.3 mL HCl (1 M)

- Na-Alg (4%)-HCl-beads = 1 mL 4% w/v Na-Alg + 0.3 mL HCl (1 M)

As expected, the FT-IR absorption spectra (1800–600 cm^{-1}) of both Na-Alg-DMSO xerogels matched the main peaks observed for Na-Alg powder, albeit with the main COO^- and C–O stretching bands (1595 cm^{-1} , 1297 cm^{-1} , respectively) slightly blue shifted (Figure S10a), suggesting the involvement in additional hydrogen bonding.⁵⁴⁻⁵⁶ On the other hand, the spectra for Na-Alg (2%)-oxalic-gel resulted from overlapping the absorption spectra from Na-Alg and oxalic acid and also showed slight blue shifts of the main bands assigned to the biopolymer, similarly to Na-Alg-DMSO samples (Figure S10b). In the case of Na-Alg (2%)- CaCl_2 used as control, no shift of the mayor bands were observed (Figure S10c). Tables S5-S7 summarize the peak assignment for all FT-IR spectra.

In order to get some insights into the microstructure of the materials, we conducted SEM of the corresponding xerogels (Figure 7 and Figure S11). A nanoporous and granular surface composed of particles between 0.1 and 0.3 μm in diameter was characteristic for the bulk Na-Alg (2%)- CaCl_2 gel (Figure 7a). Such rough surface was also observed for Na-Alg (2%)-oxalic-gel, albeit a denser network and less defined granules (Figure 7b). On the other hand, Na-Alg-DMSO xerogels showed a highly entangled fibrillar network with rope-like bundles (Figure 7c and 7d). Although we collected numerous images of the bulk samples, it should be considered that changes in the nanostructures could take place during the preparation of the samples. Thus, the conclusions derived from these images should always be interpreted cautiously.

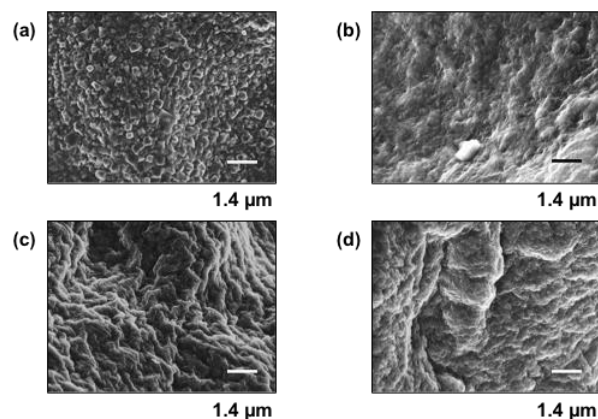


Figure 7. Selected SEM micrographs: (a) Na-Alg (2%)-CaCl₂ xerogel; (b) Na-Alg (2%)-oxalic xerogel; (c) Na-Alg (2%)-DMSO xerogels; (d) Na-Alg (4%)-DMSO xerogel.

The gel nature of the different materials and their mechanical response was studied by dynamic rheological experiments (Table 2 and Figures S12-S14). Despite the weak nature of the gels, the results showed that at the same concentration of biopolymer, the storage modulus of Na-Alg-oxalic-gel was 1.5 times higher than that of Na-Alg-DMSO, and slightly superior to Na-Alg-CaCl₂. In addition, Na-Alg-oxalic-gel showed the lowest $\tan \delta$ value and the highest yield stress γ indicating superior elasticity of this material. The damping properties of Na-Alg-oxalic-gel were close to those of Na-Alg-HCl, albeit the storage modulus of the former was ca. 2 times lower. The thermal stability (*i.e.*, the higher the T_{gel} the higher the thermal stability) of the gels prepared using DMSO, oxalic acid or maleic acid above ca. 90 °C was further confirmed by DSC and T_{gel} measurements (Figures S15-S16).

Table 2. Rheological properties of selected systems.

Gel	G' (Pa)	G'' (Pa)	$\tan \delta$	γ (%)
-----	-----------	------------	---------------	--------------

Na-Alg (2%)-DMSO	57.7	7.2	0.125	16.0
Na-Alg (4%)-DMSO	741.0	136.6	0.184	3.3
Na-Alg (2%)-Oxalic	86.3	8.1	0.094	29.2
Na-Alg (2%)-CaCl ₂	83.9	10.7	0.128	25.6
Na-Alg (2%)-HCl	180.8	19.8	0.110	20.6
Na-Alg (4%)-HCl	315.0	34.2	0.109	32.8

Moreover, the thixotropic^{57,58} behavior of Na-Alg-DMSO gels previously observed with the bulk gel (*vide supra*), was also confirmed by a 3-step loop test involving (1) application of 0.1% shear strain ($G' > G''$, gel), (2) increase of the strain to 1000% ($G' < G''$, fluid) and (3) return to the starting strain value ($G' > G''$, gel). Full recovery of the gel strength was immediately reached after each cycle (Figure 8)

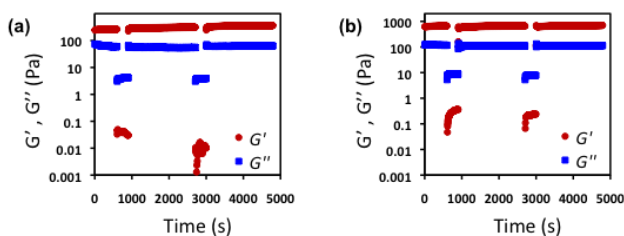


Figure 8. Thixotropic behavior of (a) Na-Alg (2%)-DMSO gel and (b) Na-Alg (4%)-DMSO gel prepared by adding 1 mL of DMSO onto 1 mL of the corresponding Na-Alg aqueous solutions. The experiments were performed at 0.1% strain and 1 Hz.

Computational studies

Na-Alg-DMSO gels. Initially, quantum mechanical calculations at the M06L/6-31+G(d,p) level were performed on small model complexes to evaluate the applicability of the “egg-box” model,

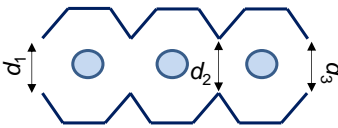
which is the most accepted description of the Ca^{2+} -containing Na-Alg hydrogels,²³⁻²⁵ to the DMSO-based gels prepared in this work. For this purpose, model chains with deprotonated carboxylate groups were constructed for Na-Alg considering two identical (M–M or G–G) or two different (M–G) residues. The M-M residues, which were considerably more stable than the M-G residues (> 30 kcal/mol), were used to build model complexes by positioning a Ca^{2+} inside the cavity defined by two properly arranged model chains. Results derived from geometry optimizations demonstrated the stability of complexes with four, or even more oxygen atoms, coordinating the single Ca^{2+} (Figure S18), which is consistent with the “egg-box”-like models confirmed experimentally²³⁻²⁵ and theoretically²⁶⁻²⁸ for Ca^{2+} -containing Na-Alg gels. Furthermore, these results were achieved considering geometry optimizations in both the gas-phase and aqueous solution.

Substitution of the Ca^{2+} cation by a DMSO molecule in these complexes resulted in a drastic destabilization after geometry optimization. Thus, the DMSO molecule was not able to compensate the repulsive interactions between the carboxylate groups of the alginate model chains, as occurred for the Ca^{2+} -containing complexes. Consequently, the distance between the two Na-Alg model chains increased during the optimizations until they separated completely.

In order to look for the interactions responsible of the stability of Na-Alg-DMSO gels, models including explicit water molecules were examined using conventional Langevin MD simulations. More specifically, the three Na-Alg-DMSO models described in the Methods (see Experimental Section), which differ in DMSO-to-water ratio, were constructed and equilibrated. Production trajectories, which took 5 ns each one, allowed us to ascertain the role of water···DMSO interactions in the cohesion of the Na-Alg chains. For this purpose, two

geometric parameters, defined as d_{av} and Δd in Table 3, were used to define the firmness of the cavity formed by the two modelled Na-Alg chains (Table 3).

Table 3. Geometric parameters used to define the cavity of Na-Alg-DMSO gels. In the scheme, blue circles indicate the center of the cavity, in which DMSO molecules were put at the beginning of the Na-Alg-DMSO/# simulations.



$$d_{av} = \frac{d_1 + d_2 + d_3}{3}$$

$$\Delta d = \text{abs}(d_3 - d_1)$$

Model	d_{av} (Å)	Δd (Å)
Na-Alg-DMSO/1	12.9 ± 2.3	8.1 ± 5.1
Na-Alg-DMSO/2	10.8 ± 0.4	0.8 ± 0.6
Na-Alg-DMSO/3	12.8 ± 1.3	3.5 ± 2.6
Na-Alg-Ox ²⁻ /1	13.3 ± 1.7	4.1 ± 2.3
Na-Alg-Ox ²⁻ /2	12.4 ± 1.1	2.7 ± 1.7
Na-Alg-OxH ⁻	12.7 ± 1.2	3.5 ± 1.8

Both d_{av} and Δd average values indicate that the cavity formed by the two Alg chains exhibit much less fluctuations when the environment is 50:50 DMSO:water, the dimensional stability of the system varying as follows: Na-Alg-DMSO/1 < Na-Alg-DMSO/3 << Na-Alg-DMSO/2. Accordingly, the co-existence of enough water and DMSO molecules seems to be a crucial factor for the formation of stable Na-Alg-DMSO gels. Visual inspection of the recorded snapshots suggested that, apparently, water molecules solvate the carboxylate groups of Alg chains while DMSO stabilizes the ionic complexes formed between Na⁺ ions and the carboxylate

groups of Alg (Figure S19). This hypothesis is fully consistent with recent studies that concluded that the solvation of metal cations is, in general, higher in DMSO than in water.⁵⁹

On the basis of these results, REMD simulations were carried out on Na-Alg-DMSO/2, 32 replicas (4 ns for each replica) being performed in a temperature range from 272 to 400.94 K. This MD based technique speeds convergence relative to brute force conventional MD. The method is based on the generation of a number of copies (“replicas”) of the system that span from the temperature of interest to heated states, which facilitates overcoming the free energy barriers. Periodic swaps of neighbouring replicas, which are performed while preserving an overall Boltzmann-weighted ensemble at each temperature (Monte Carlo based criterion of swap acceptance), enable conformations to heat up and cool down.

Stored configurations were grouped in clusters using the clustering algorithm DBSCAN,⁶⁰ which is implemented in the post-processing program *cpptraj* of the Amber package.⁶¹ Application of this algorithm, which is based on the shape defined by density of atoms of the system, considering the Na-Alg model molecules led to six different clusters with population $\geq 1.5\%$. Table 4 lists the population, the average distance between all pairs of Na-Alg atoms in the cluster (Γ) and both the d_{av} and Δd values for the representative cluster structure.

Table 4. Results derived from the clustering analysis of the structures obtained using REMD on Na-Alg-DMSO/2. Γ indicates the average distance between pairs of Na-Alg atoms in the cluster. The meaning of d_{av} and Δd values, which are taken from the representative structure of each cluster, is described in the caption of Table 3.

Cluster #	Population (%)	Γ (Å)	d_{av} (Å)	Δd (Å)
-----------	----------------	--------------	--------------	----------------

0	69.1	3.40 ± 0.88	11.1	0.3
1	1.8	1.14 ± 0.32	7.3	0.4
2	1.8	1.73 ± 0.55	14.6	9.1
3	1.8	1.51 ± 0.39	20.2	22.0
4	1.7	1.73 ± 0.42	11.6	3.8
5	1.5	1.78 ± 0.62	11.2	0.5

The most populated cluster (cluster 0), which contains almost 70%, of the stored structures, provides the most representative disposition of the Na-Alg molecules. The geometric parameters d_m and Δd values derived from the structures contained in this cluster are in very good agreement with those provided by the Na-Alg-DMSO/2 Langevin MD trajectory. Indeed, visual inspection of representative structures belonging to such cluster (Figure 9a) evidenced the co-existence of DMSO and water inside the cavity, forming hydrogen bonded networks that strongly contribute to the stabilization of the ionic complexes between charged groups. Thus, water tends to surround the carboxylate groups of the Na-Alg chain while DMSO molecules mainly interact with the Na^+ . These results support the essential role played by water molecules in the stability of Na-Alg-DMSO gels.

Na-Alg-oxalic gels. Initially, DFT calculations at the M06L/6-31+G(d,p) level were carried out to examine the influence of the oxalic acid in the stability of the “egg-box” model. For this purpose, we followed a strategy similar to that described above for Na-Alg-DMSO gels. More specifically, the Ca^{2+} cation of the stable model complexes containing two identical or different Alg residues was replaced by Ox^{2-} or OxH^- . *Geometry optimization of Ox^{2-} -containing systems led to the disruption of the complex, which was attributed to the electrostatic repulsion*

between the Ox^{2-} and the carboxylate moieties of Na-Alg. In opposition, very stable complexes were found for OxH^- (Figure S20). In these structures, the electrostatic repulsion between the negatively charged carboxylate groups of OxH^- and Alg were compensated by the simultaneous formation of three $O-H\cdots O^-$ stabilizing interactions, both OxH^- and Alg species being able to act as hydrogen donor. These results suggest that a mechanism similar to the “egg-box” one could explain the stability of Na-Alg-oxalic gels, even though the chemical nature of the interactions is completely different from that found for Na-Alg-Ca gels.

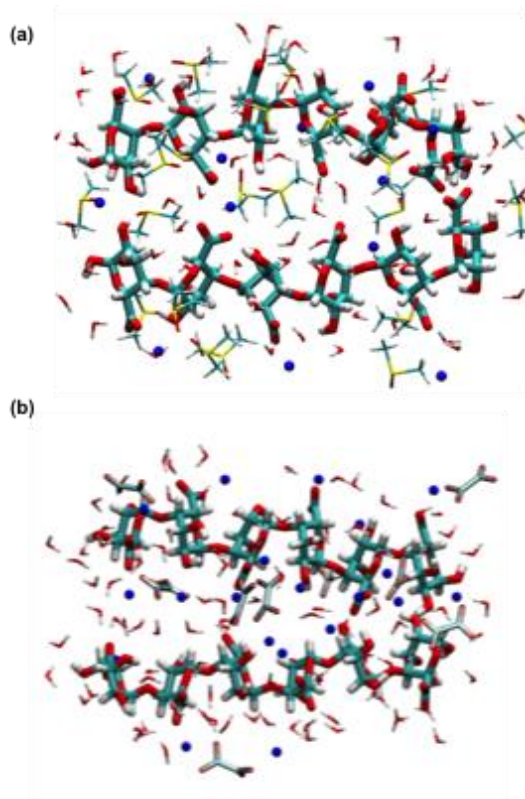


Figure 9. Representative structures of cluster 0 derived from REMD simulations for (a) Na-Alg-DMSO/2 and (b) Na-Alg-Ox2-/2 models.

Langevin MD simulations on the three models described in the Methods (see Experimental Section) were performed to get deeper understanding on the stability of Na-Alg-

oxalic gels. Such models, which differ in the number of Ox^{2-} molecules or the protonation degree of the oxalic acid, were equilibrated. Subsequent production trajectories were used to evaluate the cohesion between the Na-Alg chains through the geometric parameters d_{av} and Δd values, which were defined above.

Results, which are included in Table 3, reflect that the cavity formed by two Alg chains exhibit greater fluctuations than those previously found for Na-Alg-DMSO/2 model. These results, which are in apparent contradiction with DFT calculations, indicate that explicit water molecules soften the repulsive electrostatic repulsions between the carboxylate groups of the Alg chains and the dianion Ox^{2-} . This effect, which is not achieved when the solvent is represented as a simple dielectric medium, proves how important the explicit consideration of water molecules is in the description of hydrogels. Furthermore, both the average geometric parameters and their standard deviations suggest that the stability of the Na-Alg- Ox^{2-} models depends on the concentration of Ox^{2-} dianions.

Detailed inspection of representative snapshots indicated that the Ox^{2-} species do not interact directly with the Alg chains in Na-Alg- Ox^{2-} /1 model (Figure S21). On the contrary, the three Ox^{2-} molecules are surrounded by water molecules, forming stable hydrogen bonding networks. This feature explains the fluctuations around the averaged d_{av} and Δd values (Table 3), which are essentially due to the first hydration shell. Thus, the thermal movements inside the cavity associated to each Ox^{2-} molecules are severely affected by the fluctuations of water molecules.

On the other hand, smaller fluctuations were identified for the Na-Alg- OxH^- and Na-Alg- Ox^{2-} /2 models (Figure S22). In the former model, the OxH^- molecules form stable $\text{O}-\text{H}\cdots\text{O}^-$

interactions with the Alg chains similar to those found using DFT calculations. Although water hydrogen bonded to the OxH^- molecule still cause fluctuations in the cavity, $\text{Alg}\cdots\text{OxH}^-$ specific interactions reduce the mobility of the polymer chains and stabilize the cavity with respect to $\text{Na-Alg-Ox}^{2-}/1$. These features support the mechanism derived from DFT calculations for $\text{Na-Alg-oxalic gels}$. However, the most striking result corresponds to the $\text{Na-Alg-Ox}^{2-}/2$ model, which displayed the smallest fluctuations. Although the latter result suggests that the increment in the number of Ox^{2-} favors the formation of interactions with the Alg chains, detailed inspection of representative snapshots prove the existence of a complex and very stable network of interactions. More specifically, Alg, Ox^{2-} , water and Na^+ species form multiple interactions, the role played by the latter counterions being apparently crucial. These results are fully consistent with previously discussed experimental observations, according to which stable $\text{Na-Alg-oxalic gels}$ are formed at acid pHs. Thus, Ox^{2-} could act as cross-linkers among Na-Alg chains because of the shielding effects induced by the Na^+ counterions and water molecules that compensate the repulsive interactions between the carboxylate moieties of Alg chains and Ox^{2-} .

REMD simulations of the $\text{Na-Alg-Ox}^{2-}/2$ model confirmed this complex mechanism. Results, which are displayed in Table 5, reflect the existence of nine clusters with populations higher than 1.5%. Eight of such clusters (clusters 1-8) exhibit populations lower than 4.5%, while the cluster 0 encloses almost 50% of the saved microstructures. Moreover, the average distance between all pairs of Na-Alg atoms (Γ) is significantly higher for cluster 0 than for the other clusters, this feature being also observed for the $\text{Na-Alg-DMSO}/2$ system (Table 4). Accordingly, the most occupied cluster displays the highest spreading of Na^+ ions. This feature is particularly relevant for the Na-Al-Ox^{2-} model, which contains the highest number of Na^+

counteractions. Furthermore, the d_{av} and Δd values for cluster 0 are fully consistent with those derived from Langevin MD (Table 3).

Table 5. Results derived from the clustering analysis of the structures obtained using REMD on Na-Alg-Ox²⁻/2. Γ indicates the average distance between pairs of Na-Alg atoms in the cluster. The meaning of d_{av} and Δd values, which are taken from the representative structure of each cluster, is described in the caption of Table 3.

Cluster #	Population (%)	Γ (Å)	d_{av} (Å)	Δd (Å)
0	47.7	3.48 ± 0.91	10.6	3.9
1	4.3	1.92 ± 0.51	14.4	3.1
2	3.3	2.06 ± 0.68	12.5	4.8
3	2.8	2.18 ± 0.67	15.1	13.8
4	2.8	1.81 ± 0.65	10.5	2.3
5	2.7	1.89 ± 0.77	10.5	2.0
6	2.1	1.71 ± 0.68	11.8	1.8
7	1.9	1.50 ± 0.49	13.9	9.7
8	1.5	1.65 ± 0.58	13.4	6.9

A representative structure of cluster 0 is displayed in Figure 9b. As it can be seen, it presents a complex network of interactions, comprising Ox²⁻⋯Na⁺, Ox²⁻⋯Alg and Alg⋯Na⁺. The presence of these interactions is confirmed by the radial distribution functions displayed in Figure 10, which shows a sharp and well peak at distances lower than 2.5 Å for all pairs of above mentioned species. Moreover, water molecules, which surround charged species, prevent from

repulsive interactions between the negatively charged carboxylate groups contained in both Alg and Ox^{2-} . Overall, results obtained for Na-Alg-oxalic models indicate that the stability of the observed gels comes from a dense network of strong interactions that involve the species of the system: Alg chains, Ox^{2-} molecules, and Na^+ counterions. These interactions, which comprise charged species, are strong and very frequent. Consequently, they behave as glue keeping all the species together.

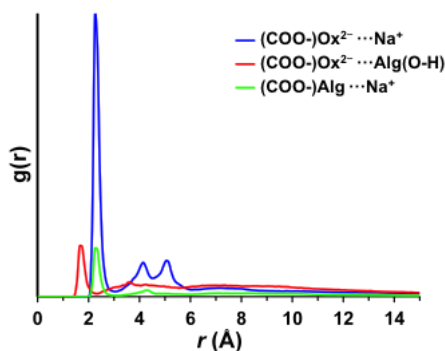


Figure 10. Radial distribution functions for pairs of interacting species (carboxylate from $\text{Ox}^{2-} \cdots \text{Na}^+$, carboxylate from $\text{Ox}^{2-} \cdots$ hydroxyl of Alg, and carboxylate from $\text{Alg} \cdots \text{Na}^+$) derived from REMD trajectories of the most populated cluster θ of Na-Alg- $\text{Ox}^{2-}/2$.

MTX-loading and release from Na-Alg gels, beads and films

Alginate-based hydrogels have been extensively used in tissue engineering^{62,63} and as drug delivery systems.⁶⁴⁻⁷² Within this context, the possibility to prepare Na-Alg-oxalic gels in different forms including beads and films (Figure S23) motivated us to evaluate their ability for the encapsulation and controlled release of a pharmaceutical compound and compare it with the classical Na-Alg- CaCl_2 gel as a control system. It is worth mentioning that the conjugate base of oxalic acid is also a competitive inhibitor of the lactate dehydrogenase (LDH) enzyme, which has been shown to inhibit tumor formation and growth.⁷³ In our study, we evaluated the

encapsulation and release of methotrexate (MTX) as model water-soluble therapeutic cargo. MTX is an anticancer drug approved for the treatment of a large variety of cancers, and has been also incorporated in a variety of gel systems.^{74,75} Light absorption of MTX does not overlap with that of oxalic acid, which makes it a good candidate for drug delivery studies. However, MTX constitutes a challenge drug model because of its known susceptibility to degrade in acidic aqueous media under light exposure and/or stored for long periods.^{76,77} Thus, the samples were covered with aluminum foil during the experiments.

UV-vis spectra of MTX dissolved in a mixture H₂O:EtOH (3:1, v/v) were recorded to build the calibration curve (Figure S24). MTX displays the maximum absorption peak at 304 nm with a shoulder at 352 nm. As oxalic acid aqueous solutions absorbs at around (and below) 300–310 nm (Figure S25a),⁷⁸ the drug-release quantification from those systems containing oxalic acid was done considering the calibration curve at 352 nm, whereas drug-release from CaCl₂-based systems was monitored at 304 nm. It is important to mention that MTX UV-vis spectra vary depending on the solvent or pH of the media, which is in agreement with the data reported in the literature^{79,80} Spectra recorded in the calibration media and oxalic acid aqueous solutions are similar (peak ca. 300 nm and shoulder at 351 nm), whereas spectra recorded in CaCl₂ aqueous solution or in water showed the absorption shoulder at ca. 370 nm (Figure S25b).

Na-Alg-oxalic-acid gels, beads and films were prepared as described in the Experimental Section, and loaded with MTX (Figure 11). The content of MTX embedded in each system corresponded to 2 mg/mL (gel), 126.6 ± 3.5 μ g/mL (film; ca. 52% loading efficiency), 29.81 ± 7.40 μ g/mL (oxalic-based beads; ca. 30% loading efficiency) and 27.20 ± 14.61 μ g/mL (CaCl₂ beads; ca. 30% loading efficiency). Cross-linking solutions were also analyzed to quantify any drug loss during the gelation process of films (Figure S25b). The analysis revealed drug loss of

0.068 mg/mL and 0.005 mg/mL when using oxalic acid and CaCl_2 as cross-linker solutions, respectively. On the other hand, analysis of the curing solutions and washing water revealed minor drug loss (1–5 $\mu\text{g/mL}$) during the preparation of the hydrogel beads (Figure S26). Moreover, no leaching of oxalic acid was detected from the bulk gels to the release medium even after 7 days. However, some leaching of oxalic acid could be observed within the first 3 h (no additional leaching occurred after this time) in the case of beads and films (Figure S27). Thus, considering the toxicity of possible oxalate salts, the bulk gels seems to be the best choice for drug delivery applications.

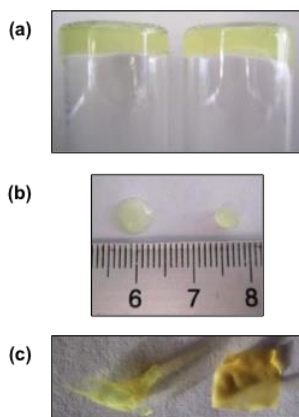


Figure 11. Representative digital photographs of MTX-loaded 2% w/v Na-Alg (a) gels, (b) beads and (c) films. In each photograph the sample on the left was prepared by using 0.5 M oxalic acid as cross-linker, whereas 0.1 M CaCl_2 was used for samples on the right.

Figure 12 displays the cumulative release profile for each system before the concentration of the drug on the release media starts to decrease presumably due to hydrolysis and/or accidental exposure to light during the analyses (Figure S28). CaCl_2 -based gels displayed a quantitative burst release within 2 h. In contrast, oxalic-based gels showed a maximum of ca. 18% drug release after 1 h. The use of oxalic-based beads allowed a maximum release of ca.

20–25% of the drug within 6 h. The best results were obtained with oxalic-based films for which a sustained MTX release up to ca. 35% within 48 h was observed. CaCl₂-based films also displayed a maximum of ca. 30–40% albeit much faster (3–6 h).

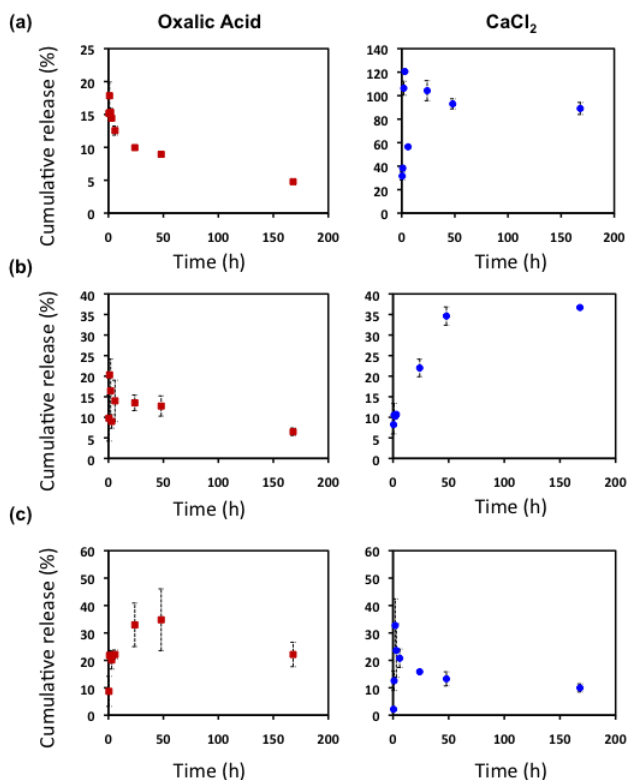


Figure 12. Release of MTX from 2% w/v Na-Alg gels (a), beads (b), and films (c) prepared using 0.5 M oxalic acid (left) or 0.1 M CaCl₂ solutions (right).

CONCLUSIONS

In conclusion, we have demonstrated the possibility to prepare rapidly Ca²⁺-free hydrogels from unmodified sodium alginate by simply mixing with small organic molecules such as polycarboxylic acid compounds as cross-linker agents instead of CaCl₂ or other metallic salts that can be potentially biotoxic if leached from the gel matrix. DMSO was also found to induce the rapid gelation of aqueous alginate solutions. The gelation process takes place at RT and

depending on the composition, gels with T_{gel} values and mechanical properties comparable to classical Ca^{2+} -containing analogs can be obtained. DMSO-based gels could support their own weight and showed thixotropic properties, which could be tuned by the biopolymer concentration. Additionally, oxalic-based gels showed superior elasticity than HCl, CaCl_2 and DMSO-based gels. In terms of gelation mechanism, computational studies revealed important differences between Na-Alg-DMSO and Na-Alg-oxalic gels. The formers are stabilized by hydrogen bonding networks between water and DMSO molecules, which in turn prefer to interact with carboxylate and Na^+ , respectively. In sharp contrast, complex ionic networks have been identified in Na-Alg-oxalic gels. In these systems, $\text{Ox}^{2-} \cdots \text{Na}^+$, $\text{Ox}^{2-} \cdots \text{Alg}$ and $\text{Alg} \cdots \text{Na}^+$ interactions play a crucial role while water molecules reduces the strength of repulsive interactions between groups with charges of the same sign. Finally, films made of alginate and oxalic acid showed good potential as synergistic anticancer drug delivery carrier. Further studies focused on this direction are currently underway in our laboratories.

ASSOCIATED CONTENT

Supporting Information. Complete experimental details, additional figures and tables. This material is available free of charge via the Internet at <http://pubs.acs.org>.

AUTHOR INFORMATION

Corresponding Author

* E-mail: carlos.aleman@upc.edu. * E-mail: David.Diaz@chemie.uni-regensburg.de; Fax: + 49 941 9434121;

Author Contributions

The manuscript was written through contributions of all authors. All authors have given approval to the final version of the manuscript.

Funding Sources

Deutsche Forschungsgemeinschaft (DFG 1748/3-1; 1748/3-2), Universität Regensburg and MINECO/FEDER (MAT2015-69367-R).

ACKNOWLEDGMENT

Financial from Deutsche Forschungsgemeinschaft (DFG 1748/3-1; 1748/3-2), Universität Regensburg and MINECO/FEDER (MAT2015-69367-R) are gratefully acknowledged. We thank Prof. Dr. A. Göpferich and his group (Universität Regensburg) for assistance with rheological measurements and Prof. Dr. Rainer Müller and Ulrike Schiebl (Universität Regensburg) for assistance with DSC measurements. C.A. is grateful to ICREA Academia program for Excellence in Research. D.D.D. thanks DFG for the Heisenberg Professorship Award. M.M.P.-M. thanks financial support through a FPI-UPC grant and a mobility DAAD Research Grant for Doctoral Candidates and Young Academics and Scientists (German Academic Exchange Service, DAAD).

REFERENCES

- (1) Smidsrod, O.; Skjak-Braek, G. Alginate as Immobilization Matrix for Cells. *Trend Biotechnol.* **1990**, *8*, 71–78.
- (2) Clark, D. E.; Green, H. C. US Patent. 2036922. 1936.
- (3) Rinaudo, M. Main Properties and Current Applications of Some Polysaccharides as Biomaterials. *Polym. Int.* **2008**, *57*, 397–430.

- (4) Qin, Y. Alginate Fibres: An Overview of the Production Processes and Applications in Wound Management. *Polym Int.* **2008**, *57*, 171–180.
- (5) Chan, L. W.; Ching, A. L.; Liew, C. V.; Heng, P. W. S. Mechanistic Study on Hydration and Drug Release Behavior of Sodium Alginate Compacts. *Drug Dev. Ind. Pharm.* **2007**, *33*, 667–676.
- (6) Draget, K. I. in *Handbook of Hydrocolloids*, G. O. Philips and P. A. Williams (Eds), Woodhead Publishing, Cambridge, pp. 379–395, 2000.
- (7) Yang, J.-S.; Xie, Y.-J.; He, W. Research Progress on Chemical Modification of Alginate: A Review. *Carbohydr. Polym.* **2011**, *84*, 33–39.
- (8) Draget, K. I.; Skjåk-Braek, G.; Smidsrød, O. Alginate Based New Materials. *Int. J. Biol. Macromolec.* **1997**, *21*, 47–55.
- (9) Tonnesen, H. H.; Karlsen, J. Alginate in Drug Delivery Systems. *Drug. Dev. Ind. Pharm.* **2002**, *28*, 621–630.
- (10) Rinaudo, M. On the Abnormal Exponents a_v and a_D in Mark Houwink Type Equations for Wormlike Polysaccharides. *Polym Bull.* **1992**, *27*, 585–589.
- (11) Lee, K. Y.; Mooney, D. J. Alginate: Properties and Biomedical Applications. *Prog. Polym. Sci.* **2012**, *37*, 106–126.
- (12) Zhao, S. P.; Cao, M. J.; Li, H.; Li L. Y.; Xu, W. L. Synthesis and Characterization of Thermo-Sensitive Semi-IPN Hydrogels Based on Poly(ethylene glycol)-co-poly(epsilon-caprolactone) Macromer, N-Isopropylacrylamide, and Sodium Alginate. *Carbohydr. Res.* **2010**, *345*, 425–431.

- (13) Sibanda, W.; Pillay, V.; Dankwerts, M. P.; Viljoen, A. M.; Van Vuuren S. F.; Riaz, A. Experimental Design for the Formulation and Optimization of Novel Cross-Linked Oilispheres Developed for In Vitro Site Specific Release of Mentha Piperita Oil. *AAPS PharmSciTech.* **2004**, *5*, 1–14.
- (14) Lee, K. Y.; Kong, H. J.; Larson, R. G.; Mooney, D. J. Hydrogel Formation via Cell Crosslinking. *Adv. Mater.* **2003**, *15*, 1828–1832.
- (15) Drury, J. L.; Boontheekul T.; Mooney, D. J. Cellular Cross-Linking of Peptide Modified Hydrogels. *J. Biomech. Eng.* **2005**, *127*, 220–228.
- (16) Pongianyakul, T.; Puttipipatkachorn, S. Modulating Drug Release and Matrix Erosion of Alginate Matrix Capsules by Microenvironmental Interaction with Calcium Ion. *Eur. J. Pharm. Biopharm.* **2007**, *67*, 187–195.
- (17) Jeon, O.; Bouhadir, K. H.; Mansour, J. M.; Alsberg, E. Photocrosslinked Alginat Hydrogels with Tunable Biodegradation Rates and Mechanical Properties. *Biomaterials* **2009**, *30*, 2724–2734.
- (18) Smeds, K. A.; Grinstaff, M. W. Photocrosslinkable Polysaccharides for In Situ Hydrogel Formation. *J. Biomed. Mater. Res.* **2001**, *54*, 115–121.
- (19) Chan, A. W.; Whitney, R. A.; Neufeld, R. J. Semisynthesis of a Controlled Stimuli-Responsive Network Alginate. *Biomacromolecules* **2009**, *10*, 609–616.
- (20) Eiselt, P.; Lee, K. Y.; Mooney, D. J. Rigidity of Two-Component Hydrogels Prepared from Alginate and Poly(ethylene glycol)-Diamines. *Macromolecules* **1999**, *32*, 5561–5566.

- (21) Lee, K. Y.; Bouhadir, K. H.; Mooney, D. J. Degradation Behavior of Covalently Cross-Linked Poly(aldehyde guluronate) Hydrogels. *Macromolecules* **2000**, *33*, 97–101.
- (22) Lee, C.; Shin, J.; Lee, J. S.; Byun, E.; Ryu, J. H.; Um, S. H.; Kim, D.-I.; Lee, H.; Cho, S.-W. Bioinspired, Calcium-Free Alginate Hydrogels with Tunable Physical and Mechanical Properties and Improved Biocompatibility. *Biomacromolecules* **2013**, *14*, 2004–2013.
- (23) Gombotz, W. R.; Wee, S. F. Protein Release from Alginate Matrices. *Adv. Drug. Deliv. Rev.* **1998**, *31*, 267–285.
- (24) Grant, G. T.; Morris, E. R.; Rees, D. A.; Smith, P. J. C.; Thom, D. Biological Interactions between Polysaccharides and Divalent Cations: The Egg-Box Model. *FEBS Lett.* **1973**, *32*, 195–198.
- (25) Braccini, I; Pérez, S. Molecular Basis of Ca²⁺-Induced Gelation in Alginates and Pectins: The Egg-Box Model Revisited. *Biomacromolecules* **2001**, *2*, 1089–1096.
- (26) Kalinichev, A. G.; Iskrenova-Tchoukova, E.; Ahn, W. Y.; Clark, M. M.; Kirkpatrick, R. J. Effects of Ca²⁺ on Supramolecular Aggregation of Natural Organic Matter in Aqueous Solutions: A Comparison of Molecular Modeling Approaches. *Geoderma*. **2011**, *169*, 27–32.
- (27) Plazinski, W.; Rudzinski, W. Molecular Modeling of Ca²⁺-Oligo(α -1-guluronate) Complexes: Toward the Understanding of the Junction Zone Structure in Calcium Alginate Gels. *Struct. Chem.* **2012**, *23*, 1409–1415.
- (28) Plazinski, W. Molecular Basis of Calcium Binding by Polyguluronate Chains. Revising the Egg-Box Model. *J. Comput. Chem.* **2011**, *32*, 2988–2995.

- (29) Wang, X.; Xu, H. Incorporation of DMSO and Dextran-40 into a Gelatin/Alginate Hydrogel for Controlled Assembled Cell Cryopreservation. *Cryobiology* **2010**, *61*, 345–351.
- (30) Stensvaag, V.; Furmanek, T.; Lønning, K.; Terzis, A. J.; Bierkvig, R.; Visted, T. Cryopreservation of Alginate-Encapsulated Recombinant Cells for Antiangiogenic Therapy. *Cell Transplant.* **2004**, *13*, 35–44.
- (31) Pawar, S. N.; Edgar, K. J. Chemical Modification of Alginates in Organic Solvent Systems. *Biomacromolecules* **2011**, *12*, 4095–4103.
- (32) Schiller, J.; Alegre-Requena, J. V.; Marqués-López, E.; Herrera, R. P.; Casanovas, J.; Alemán, C.; Díaz, D. D. Self-Assembled Fibrillar Networks of a Multifaceted Chiral Squaramide: Supramolecular Multistimuli-Responsive Alkogels. *Soft Matter* **2016**, *12*, 4361–4374.
- (33) Frisch, M. J.; Trucks, G. W.; Schlegel, H. B.; Scuseria, G. E.; Robb, M. A.; Cheeseman, J. R.; Scalmani, G.; Barone, V.; Mennucci, B.; Petersson, G. A.; Nakatsuji, H.; Caricato, M.; Li, X.; Hratchian, H. P.; Izmaylov, A. F.; Bloino, J.; Zheng, G.; Sonnenberg, J. L.; Hada, M.; Ehara, M.; Toyota, K.; Fukuda, R.; Hasegawa, J.; Ishida, M.; Nakajima, T.; Honda, Y.; Kitao, O.; Nakai, H.; Vreven, T.; Montgomery Jr., J. A.; Peralta, J. E.; Ogliaro, F.; Bearpark, M.; Heyd, J. J.; Brothers, E.; Kudin, K. N.; Staroverov, V. N.; Kobayashi, R.; Normand, J.; Raghavachari, K.; Rendell, A.; Burant, J. C.; Iyengar, S. S.; Tomasi, J.; Cossi, M.; Rega, N.; Millam, J. M.; Klene, M.; Knox, J. E.; Cross, J. B.; Bakken, V.; Adamo, C.; Jaramillo, J.; Gomperts, R.; Stratmann, R. E.; Yazyev, O.; Austin, A. J.; Cammi, R.; Pomelli, C.; Ochterski, J. W.; Martin, R. L.; Morokuma, K.; Zakrzewski, V. G.; Voth, G. A.; Salvador, P.; Dannenberg, J. J.; Dapprich, S.;

Daniels, A. D.; Farkas, O.; Foresman, J. B.; Ortiz, J. V.; Cioslowski, J.; Fox, D. J. Gaussian 09, Revision A.02. Gaussian Inc. 2009.

(34) Zhao, Y.; Truhlar, D. G. The M06 Suite of Density Functionals for Main Group Thermochemistry, Thermochemical kinetics, Noncovalent Interactions, Excited States, and Transition Elements: Two New Functionals and Systematic Testing of Four M06-Class Functionals and 12 Other Functionals. *Theor. Chem. Acc.* **2008**, *120*, 215–241.

(35) Zhao, Y.; Truhlar, D. G. A New Local Density Functional for Main-Group Thermochemistry, Transition Metal Bonding, Thermochemical Kinetics, and Noncovalent Interactions. *J. Chem. Phys.* **2006**, *125*, 194101.

(36) Tomasi, J.; Persico, M. Molecular Interactions in Solution: An Overview of Methods Based on Continuous Distributions of the Solvent. *Chem. Rev.* **1994**, *94*, 2027–2094.

(37) Phillips, J. C.; Braun, R.; Wang, W.; Gumbart, J.; Tajkhorshid, E.; Villa, E.; Chipot, C.; Skeel, R. D.; Kale, L.; Schulten, K. Scalable Molecular Dynamics with NAMD. *J. Comput. Chem.* **2005**, *26*, 1781–1802.

(38) Cornell, W. D.; Cieplak, P.; Bayly, C. I.; Gould, I. R.; Merz, K. M.; Ferguson, D. M.; Spellmeyer, D. C.; Fox, T.; Caldwell, J. W.; Kollman, P. A. A Second Generation Force Field for the Simulation of Proteins, Nucleic Acids, and Organic Molecules. *J. Am. Chem. Soc.* **1995**, *117*, 5179–5197.

(39) Kirschner, K. N.; Yongye, A. B.; Tschampel, S. M.; Daniels, C. R.; Foley, B. L.; Woods, R. J. GLYCAM06: A Generalizable Biomolecular Force Field. Carbohydrates. *J. Comput. Chem.* **2008**, *29*, 622–655.

- (40) Jorgensen, W. L.; Chandrasekhar, J.; Madura, J. D.; Impey, R. W.; Klein, M. L. Comparison of Simple Potential Functions for Simulating Liquid Water. *J. Chem. Phys.* **1983**, *79*, 926–935.
- (41) Fox, T.; Kollman, P. A. Application of the RESP Methodology in the Parametrization of Organic Solvents. *J. Phys. Chem. B.* **1998**, *102*, 8070–8079.
- (42) Wang, J.; Wolf, R. M.; Caldwell, J. W.; Case, D. A. Development and Testing of a General Amber Force Field. *J. Comput. Chem.* **2004**, *25*, 1157–1174.
- (43) Ryckaert, J.-P.; Ciccotti, G.; Berendsen, H. J. C. Numerical Integration of the Cartesian Equations of Motion of a System with Constraints: Molecular Dynamics of *n*-Alkanes. *J. Comput. Phys.* **1977**, *23*, 327–341.
- (44) Toukmaji, A.; Sagui, C.; Board, J.; Darden, T. Efficient Particle-Mesh Ewald Based Approach to Fixed and Induced Dipolar Interactions. *J. Chem. Phys.* **2000**, *113*, 10913–10927.
- (45) Plazinski, W. Molecular Basis of Calcium Binding by Polyguluronate Chains. Revising the Egg-Box Model. *J. Comput. Chem.* **2011**, *32*, 2988–2995.
- (46) Berendsen, H. J. C.; Postma, J. P. M.; Vangunsteren, W. F.; Dinola, A.; Haak, J. R. Molecular Dynamics with Coupling to an External Bath. *J. Chem. Phys.* **1984**, *81*, 3684–3690.
- (47) Pérez-Madrigal, M. M.; Estrany, F.; Armelin, E.; Díaz, D. D.; Alemán, C. Current Status and Challenges of Biohydrogels for Applications as Supercapacitors and Secondary Batteries. *J. Mater. Chem. A.* **2016**, *4*, 1792–1805.
- (48) Rochas, C.; Brûlet, A.; Guenet, J. M. Thermoreversible Gelation of Agarose in Water Dimethyl-Sulfoxide Mixtures. *Macromolecules* **1994**, *27*, 3830–3835.

- (49) Östlund, Å.; Lundberg, D.; Nordstierna, L.; Holmberg, K.; Nydén, M. Dissolution and Gellation of Cellulose in TBAF/DMSO Solutions: The Role of Fluoride Ions and Water. *Biomacromolecules* **2009**, *10*, 2401–2407.
- (50) Watase, M.; Nishinari, K. Effects of PH and DMSO Content on the Thermal and Rheological Properties of High Methoxyl Pectin-Water Gels. *Carbohydr. Polym.* **1993**, *20*, 175–181.
- (51) S. M. Prabhu, S. M.; Meenakshi, S. Novel One-Pot Synthesis of Dicarboxylic Acids Mediated Alginate-Zirconium Biopolymeric Complex for Defluoridation of Water. *Carbohydr. Polym.* **2015**, *120*, 60–68.
- (52) Gyawali, D.; Nair, P.; Zhang, Y.; Tran, R. T.; Zhang, C.; Samchukov, M.; Makarov, M.; Kim, H. K. W.; Yang, J. Citric Acid-Derived In Situ Crosslinkable Biodegradable Polymers for Cell Delivery. *Biomaterials* **2010**, *31*, 9092–9105.
- (53) Stone, S. A.; Gosavi, P.; Athauda, T. J.; Ozer, R. R. In Situ Citric Acid Crosslinking of Alginate/Polyvinyl Alcohol Electrospun Nanofibers. *Mater. Lett.* **2013**, *112*, 32–35.
- (54) Lawrie, G.; Keen, I.; Drew, B.; Chandler-Temple, A.; Rintoul, L.; Fredericks, P.; Grøndahl, L. Interactions Between Alginate and Chitosan Biopolymers Characterized Using FTIR and XPS. *Biomacromolecules* **2007**, *8*, 2533–2541.
- (55) Pereira, L.; Sousa, A.; Coelho, H.; Amado, A. H.; Ribeiro-Claro, P. J. Use of FTIR, FT-Raman and ¹³C-NMR Spectroscopy for Identification of Some Seaweed Phycocolloids. *Biomol. Eng.* **2003**, *20*, 223–228.

- (56) Sartori, C.; Finch, D. S.; Ralph, B.; Gilding, K.; Determination of the Cation Content of Alginate Thin Films by FTIR Spectroscopy. *Polymer* **1997**, *38*, 43–51.
- (57) Kirilov, P.; Gauffre, F.; Franceschi-Messant, S.; Perez, E.; Rico-Lattes, I. Rheological Characterization of a New Type of Colloidal Dispersion Based on Nanoparticles of Gelled Oil. *J. Phys. Chem. B.* **2009**, *113*, 11101–11108.
- (58) Nagarajan, S. A Renewable Resource-Derived Thixotropic Self-Assembled Supramolecular Gel: Magnetic Stimuli Responsive and Real-Time Self-Healing Behavior. *RSC Adv.* **2015**, *5*, 77589–77594.
- (59) Di Bernardo, P.; Zanonato, P. L.; Benetollo, F.; Melchior, A.; Tolazzi, M.; Rao, L. Energetics and Structure of Uranium(VI)–Acetate Complexes in Dimethyl Sulfoxide. *Inorg. Chem.* **2012**, *51*, 9045–9055.
- (60) Ester, M.; Kriegel, H.-P.; Sander, J.; Xu, X. Proceedings of the Second International Conference on Knowledge Discovery and Data Mining (KDD-96), 1996, pp 226–231.
- (61) Case, D. A.; Darden, T. A.; Cheatham, I.; Simmerling, C. L.; Wang, J.; Duke, R. E.; Luo, R.; Walker, R. C.; Zhang, W.; Merz, K. M.; Roberts, B.; Hayik, S.; Roitberg, A.; Seabra, G.; Swails, J.; Goetz, A. W.; Kolossváry, I.; Wong, K. F.; Paesani, F.; Vanicek, J.; Wolf, R. M.; Liu, J.; Wu, X.; Brozell, S. R.; Steinbrecher, T.; Gohlke, H.; Cai, Q.; Ye, X.; Wang, J.; Hsieh, M.-J.; Cui, G.; Roe, D. R.; Mathews, D. H.; Seetin, M. G.; Salomon-Ferrer, R.; Sagui, C.; Babin, V.; Luchko, T.; Gusarov, S.; Kovalenko, A.; Kollman, P. A. AMBER 12, University of California: San Francisco, 2012.

- (62) Lee, K. Y.; Mooney, D. J. Hydrogels for Tissue Engineering. *Chem. Rev.* **2001**, *101*, 1869–1880.
- (63) Augst, A. D.; Kong, H. J.; Mooney, D. J. Alginate hydrogels as biomaterials. *Macromol Biosci.* **2006**, *6*, 623–633.
- (64) Jain, D.; Bar-Shalom, D. Alginate Drug Delivery Systems: Application in Context of Pharmaceutical and Biomedical Research. *Drug Dev. Ind. Pharm.* **2014**, *40*, 1576–1584.
- (65) Pegg, C. E.; Jones, G. H.; Athauda, T. J.; Ozer, R. R.; Chalker, J. M. Facile Preparation of Ammonium Alginate-Derived Nanofibers Carrying Diverse Therapeutic Cargo. *Chem. Commun.* **2014**, *50*, 156–158.
- (66) Gonçalves, M.; Figueira, M.; Maciel, D.; Rodrigues, J.; Shi, X.; Tomás, H.; Li, Y. Antitumor Efficacy of Doxorubicin-Loaded Laponite/Alginate Hybrid Hydrogels. *Macromol. Biosci.* **2014**, *14*, 110–120.
- (67) Paradee, N.; Sirivat, A.; Niamlang, S.; Prissanaroon-Ouajai, W. Effects of Crosslinking Ratio, Model Drugs, and Electric Field Strength on Electrically Controlled Release for Alginate-Based Hydrogel. *J. Mater. Sci. Mater. Med.* **2012**, *23*, 999–1010.
- (68) Mandal, S.; Basu, S. K.; Sa, B. Ca²⁺ Ion Cross-Linked Interpenetrating Network Matrix Tablets of Polyacrylamide-Grafted-Sodium Alginate and Sodium Alginate for Sustained Release of Diltiazem Hydrochloride. *Carbohydr. Polym.* **2010**, *82*, 867–873.
- (69) Chang, C. H.; Lin, Y. H.; Yeh, C. L.; Chen, Y. C.; Chiou, S. F.; Hsu, Y. M.; Chen, Y. S.; Wang, C. C. Nanoparticles Incorporated in PH-Sensitive Hydrogels as Amoxicillin Delivery for Eradication of Helicobacter Pylori. *Biomacromolecules* **2010**, *11*, 133–142.

- (70) Lucinda-Silva, R. M.; Salgado, H. R. N.; Evangelista, R. C. *Carbohydr. Polym.* Alginate-Chitosan Systems: In Vitro Controlled Release of Triamcinolone and In Vivo Gastrointestinal Transit. **2010**, *81*, 260–268.
- (71) Wang, F.-Q.; Li, P.; Zhang, J.-P.; Wang, A.-Q.; Wei, Q. A Novel PH-Sensitive Magnetic Alginate-Chitosan Beads for Albendazole Delivery. *Drug Dev. Ind. Pharm.* **2010**, *36*, 867–877.
- (72) Zhang, X.; Hui, Z.; Wan, D.; Huang, H.; Huang, J.; Yuan, H.; Yu, J. H. Alginate Microsphere Filled with Carbon Nanotube as Drug Carrier. *Int. J. Biol. Macromol.* **2010**, *47*, 389–395.
- (73) Le, A.; Charles, C.; Gouw, A.; Dinavahi, R.; Maitra, A.; Deck, L.; Royer, R.; Jagt, D. V.; Semenza, G.; Dang, C. Inhibition of Lactate Dehydrogenase A Induces Oxidative Stress and Inhibits Tumor Progression. *Proc. Natl. Acad. Sci., U.S.A.* **2009**, *107*, 2037–2042.
- (74) Liu, C.; Zhang, Z.; Liu, X.; Ni, X.; Li, J. Gelatin-Based Hydrogels with β -Cyclodextrin as a Dual Functional Component for Enhanced Drug Loading and Controlled Release. *RSC Adv.* **2013**, *3*, 25041–25049.
- (75) Bouhadir, K. H.; Alsberg, E.; Mooney, D. J. Hydrogels for Combination Delivery of Antineoplastic Agents. *Biomaterials* **2001**, *22*, 2625–2633.
- (76) Sabry, S. M.; Abdel-Hady, M.; Elsayed, M.; Fahmy, O. T.; Maher, H. M. Study of Stability of Methotrexate in Acidic Solution Spectrofluorimetric Determination of Methotrexate in Pharmaceutical Preparations Through Acid-Catalyzed Degradation Reaction. *J. Pharm. Biomed. Anal.* **2003**, *32*, 409–423.

(77) Limelette, N.; Ferry, M.; Branger, S.; Thuillier, A.; Fernandez, C. In Vitro Stability Study of Methotrexate in Blood and Plasma Samples for Routine Monitoring. *Ther. Drug Monit.* **2003**, *25*, 81–87.

(78) Lund Myhre, C. E.; Nielsen, C. J. Optical Properties in the UV and Visible Spectral Region of Organic Acids Relevant to Tropospheric Aerosols. *Atmos. Chem. Phys.* **2004**, *4*, 1759–2004.

(79) Zhang, L.; Su, T.; He, B.; Gu, Z. Self-Assembly Polyrotaxanes Nanoparticles as Carriers for Anticancer Drug Methotrexate Delivery. *Nano-Micro Lett.* **2014**, *6*, 108–115.

(80) Haijian, R.; Tavakol, M. Interaction of Anticancer Drug Methotrexate with DS-DNA Analyzed by Spectroscopic and Electrochemical Methods. *E-J. Chem.* **2012**, *9*, 471–480.

Challenging conventional wisdom: The replacement of divalent metals by small organic molecules such as polycarboxylic acids or dimethyl sulfoxide enables the preparation of metal-free alginate hydrogels.

